

Design and Evaluation of a Planar Single-Channel Shim Coil for a Permanent Magnetic Resonance Imaging Magnet

Daiki Tamada*, Yasuhiko Terada, and Katsumi Kose

Institute of Applied Physics, University of Tsukuba, Tsukuba, Ibaraki 305-8573, Japan

Received April 26, 2011; accepted May 18, 2011; published online June 1, 2011

We propose a straightforward method of designing a planar single-channel shim coil for magnetic resonance imaging (MRI) using a narrow-gap permanent magnet. The design method is based on the superposition of the current densities produced by planar second-order shim coil elements and optimization of the coefficients used for the superposition. The magnetic field homogeneity was improved from 13 to 3.3 ppm (root mean square) in the central spherical area (diameter = 18 mm), revealing that the planar single-channel shim coil is a useful device for narrow-gap permanent MRI magnets. © 2011 The Japan Society of Applied Physics

In most nuclear magnetic resonance (NMR) or magnetic resonance imaging (MRI) systems, magnetic field shimming is required to achieve field homogeneity on the order of 1 ppm. There are two types of shimming, passive and active. Passive shimming corrects magnetic field inhomogeneity (ΔB_z) by positioning pieces of magnetic material around the magnet.¹⁾ In contrast, active shimming corrects ΔB_z using shim coils.²⁾ Since ΔB_z can be expressed as the superposition of some orthogonal set of spatial functions, such as spherical harmonics, each shim coil is typically designed to generate a magnetic field corresponding to one of the spherical harmonics.³⁻⁵⁾ Therefore, active shimming is usually performed with a number of shim coils to correct spatially complicated inhomogeneity in a magnetic field.

However, such multicoil shimming has several disadvantages, namely, it reduces the available space in the magnet, consumes excessive power, and requires a large number of power supplies. To overcome these problems, our group has proposed a single-channel shim coil to correct ΔB_z using a target field approach.⁶⁾ However, the target field calculation is not straightforward because it usually requires a long trial-and-error process to optimize several parameters. Here, we propose a simple and straightforward method of designing a planar single-channel shim coil for a permanent magnet and evaluate its usefulness through its implementation.

Magnetic field inhomogeneity ($\Delta B_z = B_z - B_0$, where B_z is the z component of the magnetic field, and B_0 is the homogeneous magnetic field) can be represented as the superposition of spherical harmonics of the form:

$$\Delta B_z = \sum_{n=1}^{\infty} \sum_{m=0}^n H_{nm} T_{nm}, \quad (1)$$

$$T_{nm} = r^n P_{nm}(\cos \theta) \cos[m(\phi - \sigma_{nm})], \quad (2)$$

where T_{nm} and H_{nm} are the spherical harmonics of phase σ_{nm} and their amplitudes, respectively.⁴⁾ Anderson proposed a design method for biplanar shim coils to produce magnetic field components proportional to such spherical harmonics.³⁾ He proposed wire patterns composed of squares and circles for first- and second-order shim coils corresponding to spherical harmonics.

In our method, we represent the current density \mathbf{J}_s for a single-channel shim coil as the superposition of the second order shim coil current densities \mathbf{J}_i , as follows:

$$\mathbf{J}_s(\mathbf{r}) = \sum_i c_i \mathbf{J}_i, \quad (3)$$

where c_i is the coefficient of \mathbf{J}_i and i represents $2Z^2 - X^2 - Y^2$, $X^2 - Z^2$, $Y^2 - Z^2$, XY , YZ , or ZX . Since \mathbf{J}_i are current densities produced by thin and straight wires, which generate very high current densities, \mathbf{J}_s should be convolved with a Gaussian function to avoid abrupt changes in the current direction and undesirable higher-order spatial components of the magnetic field. However, the determination of c_i becomes nonlinear optimization problem due to this convolution. Therefore, we used a genetic algorithm⁷⁾ so as to minimize the inhomogeneity of the magnetic field with the fitness function f :

$$f = \sqrt{\frac{\int (\Delta B_z + B_s)^2 dV}{V}}, \quad (4)$$

where V is the volume of the area evaluated and B_s is the magnetic field induced by \mathbf{J}_s . The winding pattern for \mathbf{J}_s can be calculated using the stream function method.^{8,9)}

A permanent magnet MRI system was used to design and evaluate the single-channel shim coil developed in this study. The MRI system consisted of a small yokeless permanent magnet (field strength = 1.04 T, size = 238 × 184 × 252 mm³, gap width = 40 mm, weight = 85 kg; NEOMAX Engineering), a planar gradient coil set, a radiofrequency (RF) probe with a solenoid coil, and an MRI console. The whole system, except the MRI console, was installed in a variable-temperature thermostatic bath (inner size = 620 mm (W) × 340 mm (D) × 1154 mm (H), Fukushima Industries FMU-263I). The MRI console was placed next to the thermostatic bath in an area at room temperature, and the control and signal lines were connected to the gradient and RF coils through a hole in the wall of the thermostatic bath. The temperature of the thermostatic bath could be maintained between −15 and +50 °C.

The RF probe box (30 mm thickness) made of brass plates, the three-channel planar gradient coil set (a pair of 3-mm-thick gradient coil units), and the single-channel shim coil (the pair of ~2-mm-thick shim coil units described in described in this letter) were installed in the 40 mm gap in the magnet. The details of the MRI system are given elsewhere.¹⁰⁾

The magnetic field distribution was measured using a three-dimensional (3D) lattice phantom and 3D spin echo imaging sequences at −5 °C. This temperature was selected because it caused the magnetic field inhomogeneity to increase considerably compared with that at room temperature.

The phantom consisted of 11 acrylic discs (diameter = 23.9 mm, thickness = 3.0 mm) with square trenches

*E-mail address: tamada@mrlab.frsc.tsukuba.ac.jp

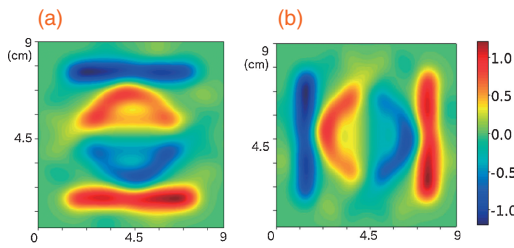


Fig. 1. Current density distributions of the single-channel shim coil: (a) J_x and (b) J_y .

(width = 1.0 mm, depth = 1.0 mm, interval = 3.0 mm) stacked in a cylindrical container (inner diameter = 24.0 mm, outer diameter = 26.2 mm, length = 62.0 mm) filled with baby oil.¹¹⁾ The 3D images of the phantom were measured using 3D spin echo (SE) sequences [repetition time (TR) = 100 ms, echo time (TE) = 12 ms, matrix = 256^3 , voxel size = $(125 \mu\text{m})^3$] with positive and negative readout gradients.

The spatial coordinates of the vertex points of the square lattices in the images were detected with a graphical user interface program. The magnetic field inhomogeneity ΔB_z at the vertex points in the central cubic area [$(18 \text{ mm})^3$] was calculated from the positional shifts of the vertices along the readout direction. Then, ΔB_z was approximated using up to fourth-order polynomials at the Cartesian coordinates. These polynomials were used for both to design the shim coil and to evaluate the magnetic field inhomogeneity.

We optimized c_i for the magnetic field inhomogeneity ΔB_z measured in the central spherical area (diameter = 18 mm) using the fitness function described in eq. (4). We did not use terms proportional to YZ and ZX because our computation time was restricted. Figure 1 shows the optimized current density distribution obtained for \mathbf{J}_s of the single-channel shim coil in a $9 \times 9 \text{ cm}^2$ area.

Figure 2(a) shows the stream function ψ for \mathbf{J}_s and the contour lines corresponding to the wire pattern of the shim coil. Figure 2(b) shows one side of the single-channel shim coil fabricated on a fiber-reinforced plastic plate ($90 \times 90 \text{ mm}^2$, 0.5 mm thick) using a polyethylene-coated copper wire (0.4 mm in diameter). Since the thickness of one side of the shim coil was less than 2 mm, the shim coil set was successfully installed in the narrow gap of the magnet together with the RF probe box and the gradient coil set, and connected to a constant-current power supply.

Figure 3(a) shows the magnetic field distributions in the xy plane at $z = 0 \text{ mm}$ and in the xz plane at $y = 0 \text{ mm}$ measured without shimming. A large magnetic field inhomogeneity is clearly seen. Figure 3(b) shows the magnetic field distributions in the same planes *calculated* using the measured magnetic field inhomogeneity and the single-channel shim coil with the optimized current. It is clear that the magnetic field inhomogeneity will be drastically reduced using the shim coil. The magnetic field calculation shows that the inhomogeneity in the central spherical area (diameter = 18 mm) will be improved from 13 ppm [root mean square: (RMS)] and 73 ppm [peak-to-peak: (P-P)] to 3.4 ppm and 60 ppm, respectively.

Figure 4(a) shows the RMS of the magnetic field inhomogeneity measured in the central spherical area plotted

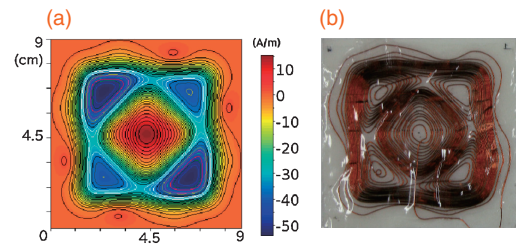


Fig. 2. (a) Stream function ψ of \mathbf{J}_s . (b) Single-channel shim coil wound on an FRP plate.

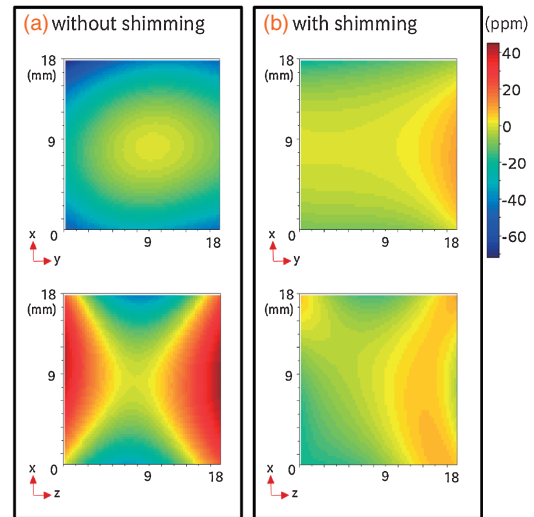


Fig. 3. Magnetic field distribution (a) without and (b) with shimming. Upper images are those in the xy plane at $z = 9 \text{ mm}$. Lower images are those in the xz plane at $y = 9 \text{ mm}$.

against the current from the power supply for the shim coil. This figure clearly shows that the inhomogeneity has a minimum at around 300 mA. At this point, the magnetic field inhomogeneity was 3.3 ppm (RMS) and 29 ppm (P-P). These values agree well with those predicted by the calculation.

Figures 4(b)–4(d) show the coefficients of the polynomials used to fit the magnetic field plotted against the current from the power supply for the shim coil. As shown in Figs. 4(b) and 4(c), the coefficients for x^2 , y^2 , z^2 , and xy change linearly with the current and become zero at around 300 mA. This result clearly shows that the single-channel shim coil works very well as a set of multiple shim coils. Conversely, the coefficients for yz and zx do not change linearly, because the corresponding shim coil elements were not used for the design of the single-channel shim coil. Figure 4(d) shows the coefficients for the third- and fourth-order polynomials, the amplitudes of which are very small.

Figure 5 shows 2D slices selected from the 3D image datasets of the 3D lattice phantom acquired with and without shimming. The images without shimming show considerable distortion along the readout direction, which originates from the magnetic field inhomogeneity, and this is dramatically reduced by shimming.

As shown in Fig. 4(a), an improvement of about threefold in the magnetic field homogeneity was achieved using the single-channel shim coil. However, about 3 ppm (RMS) inhomogeneity still remained. We attribute this residual

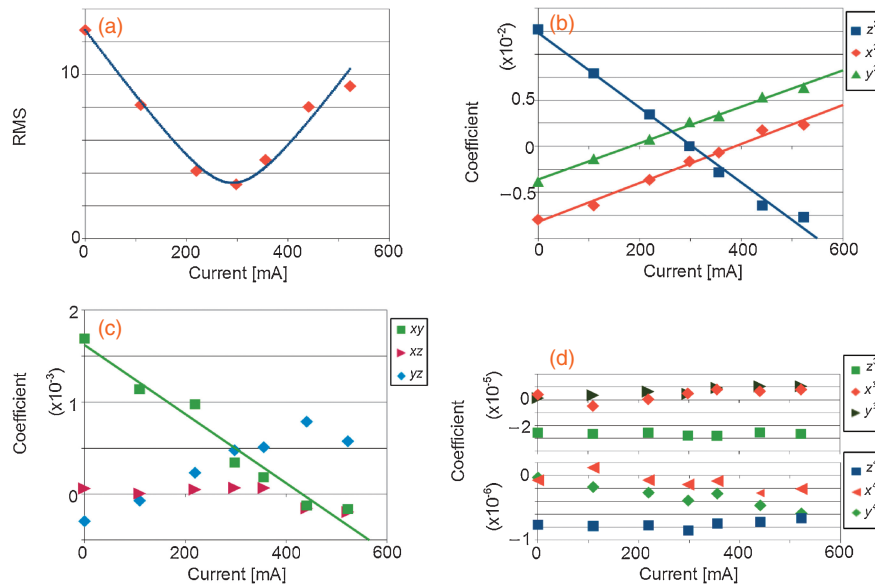


Fig. 4. (a) Magnetic field inhomogeneity plotted against electrical current for the shim coil. Magnetic field inhomogeneity fitting coefficients for polynomials plotted against the shim coil current (b) for x^2 , y^2 , and z^2 , (c) for xy , yz , and zx , and (d) for x^3 , y^3 , and z^3 , and x^4 , y^4 , and z^4 .

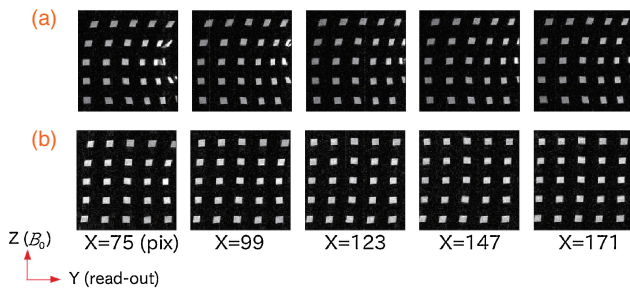


Fig. 5. 2D slices selected from 3D image datasets of the 3D lattice phantom acquired (a) without and (b) with shimming.

inhomogeneity primarily to the fact that inhomogeneity proportional to x^2 , y^2 , and z^2 does not become zero at the same current value (~ 300 mA), as shown in Fig. 4(b). If the design and fabrication of the single-channel shim coil had been perfect, x^2 , y^2 , and z^2 would have been zero at the same current value and the inhomogeneity would have improved remarkably.

We did not include second-order shim coils proportional to yz and zx because the inhomogeneity proportional to these functions was small and the computation time for optimization was limited. We also did not include higher-order terms, such as the third- and fourth-order terms. We think that the residual inhomogeneity (3 ppm RMS) may have been partly caused by those terms. However, if we use these terms to design the single-channel shim coil, more precise magnetic field distribution measurements will be required.

As is well known, a conventional shim coil set has another important function that can correct magnetic field inhomogeneity caused by the magnetic susceptibility distribution of the sample itself. The single-channel shim coil does not have this function. However, if some specific object such as a human head is frequently measured using an MRI system, another single-channel shim coil that can correct the inhomogeneous magnetic field caused by the human head can be designed.

In this study, we designed a planar single-channel shim coil for permanent magnets. However, if we use cylindrical shim coil elements for the base functions, we can design a cylindrical single-channel shim coil. Therefore, in a future work, we will design and fabricate a cylindrical single-channel shim coil for a superconducting magnet with a cylindrical bore.

In this study, we have proposed a simple and straightforward method of designing a planar single-channel shim coil for a permanent MRI magnet. Our method is based on the superposition of the current densities produced by higher-order shim coils and optimization of the coefficients for their superposition using a genetic algorithm. We designed and fabricated a single-channel shim coil for a 1.0 T permanent magnet with a 40 mm gap based on the measured magnetic field using second-order shim coil elements. By optimizing the electrical current for the shim coil, we achieved an improvement of about threefold in the magnetic field homogeneity in the central spherical area (diameter = 18 mm). Therefore, we conclude that the single-channel shim coil is a useful device for narrow-gap permanent magnets.

Acknowledgment We acknowledge Mr. R. Shigeki for his contribution to the early stage of this research.

- 1) D. I. Hoult and D. Lee: *Rev. Sci. Instrum.* **56** (1985) 131.
- 2) M. J. E. Golay: *Rev. Sci. Instrum.* **29** (1958) 313.
- 3) W. A. Anderson: *Rev. Sci. Instrum.* **32** (1961) 241.
- 4) F. Romeo and D. I. Hoult: *Magn. Resonance Med.* **1** (1984) 44.
- 5) J. Jianming: *Electromagnetic Analysis and Design in Magnetic Resonance Imaging* (CRC Press, Boca Raton, FL, 1998) p. 68.
- 6) R. Shigeki and K. Kose: Proc. 18th Int. Soc. Magnetic Resonance in Medicine, 2010, p. 1542.
- 7) D. E. Goldberg: *Genetic Algorithms in Search, Optimization and Machine Learning* (Addison-Wesley, Boston, MA, 1989) Chap. 3, p. 59.
- 8) W. A. Edelstein and F. Schenk: US Patent 4,840,700 (1989).
- 9) M. A. Martens, L. S. Petropoulos, R. W. Brown, and J. H. Andrews: *Rev. Sci. Instrum.* **62** (1991) 2639.
- 10) K. Kose: in *NMR Imaging in Chemical Engineering*, ed. S. Stapf and S.-I. Han (Wiley-VCH, Weinheim, 2006) p. 77.
- 11) S. Adachi, T. Ozeki, R. Shigeki, S. Handa, K. Kose, T. Haishi, and M. Aoki: *Rev. Sci. Instrum.* **80** (2009) 054701.